Dalton Transactions

ROYAL SOCIETY OF CHEMISTRY

PAPER

View Article Online
View Journal | View Issue

Cite this: *Dalton Trans.*, 2023, **52**, 4028

Distal scaffold flexibility accelerates ligand substitution kinetics in manganese(I) tricarbonyls: flexible thianthrene *versus* rigid anthracene scaffolds†

Jordan Labrecque, Yae-In Cho, Daniel K. McIntosh, Faridat Agboola and Michael J. Rose *

This work investigates the effect of molecular flexibility on fundamental ligand substitution kinetics in a pair of manganese(I) carbonyls supported by scaffold-based ligands. In previous work, we reported that the planar and rigid, anthracene-based scaffold with two pyridine 'arms' (**Anth-py$_2$**, **2**) serves as a bidentate, *cis* donor set, akin to a strained bipyridine (bpy). In the present work, we have installed a more flexible and dynamic scaffold in the form of thianthrene (**Thianth-py$_2$**, **1**), wherein the scaffold in the free ligand exhibits a ~130° dihedral angle in the solid state. **Thianth-py$_2$** also exhibits greater flexibility (molecular motion) in solution compared with **Anth-py$_2$**, as evidenced by longer ^{1}H NMR T_1 times **Thianthy-py$_2$** (T_1 = 2.97 s) *versus* **Anth-py$_2$** (T_1 = 1.91 s). Despite the exchange of rigid **Anth-py2** for flexible **Thianth-py2** in the complexes [(**Anth-py$_2$**)Mn(CO)$_3$Br] (**4**) and [(**Thianth-py$_2$**)Mn(CO)$_3$Br] (**3**), respectively, nearly identical electronic structures and electron densities were observed at the Mn center: the IR of **3** exhibits features at 2026, 1938 and 1900 cm^{-1}, nearly identical to the features of the anthracene-based congener (**4**) at 2027, 1936 and 1888 cm^{-1}. Most importantly, we assessed the effect of ligand-scaffold flexibility on reactivity and measured the rates of an elementary ligand substitution reaction. For ease of IR study, the corresponding halide-abstracted, nitrile-bound (PhCN) cations [(**Thianth-py$_2$**)Mn(CO)$_3$(PhCN)](BF$_4$) (**6**) and [(**Anth-py$_2$**)Mn(CO)$_3$(PhCN)](BF$_4$) (**8**) were generated *in situ*, and the PhCN → Br$^-$ back-reaction was monitored. The more flexible **3** (thianth-based) exhibited ~3–4× faster ligand substitution kinetics ($k_{25\ C}$ = 22 × 10^{-2} min^{-1}, $k_{0\ C}$ = 43 × 10^{-3} min^{-1}) than the rigid analogue **4** (anth-based: ($k_{25\ C}$ = 6.0 × 10^{-2} min^{-1}, $k_{0\ C}$ = 9.0 × 10^{-3} min^{-1}) on all counts. Constrained angle DFT calculations revealed that despite large changes in the thianthrene scaffold dihedral angle, the bond metrics of **3** about the metal center remain unchanged; *i.e.* the 'flapping' motion is strictly a second coordination sphere effect. These results suggest that the local environment of molecular flexibility plays a key role in determining reactivity at the metal center, which has essential implications for understanding the reactivity of organometallic catalysts and metalloenzyme active sites. We propose that this molecular flexibility component of reactivity can be considered a thematic 'third coordination sphere' that dictates metal structure and function.

Received 16th December 2022,
Accepted 23rd February 2023

DOI: 10.1039/d2dt04048d

rsc.li/dalton

Introduction

Basolo & Pearson's seminal 1965 publication of *Inorganic Reaction Mechanisms* detailed the governing parameters for substitution reactions of coordination complexes based on crystal field theory (CFT) arguments, providing a foundation for inorganic chemists to quantitatively explore the kinetics, thermodynamics and mechanisms of ligand exchange reactions.[1] Although elementary, ligand substitution reactions underpin a variety of important processes in materials and inorganic complexes such as catalysis, sensing and pharmacoefficacy. Basolo & Pearson's book systematically detailed the geometric (10Dq arguments), chelate and thermodynamic effects on ligand substitution kinetics. In the ensuing decades, many other factors were identified that substantially effect ligand substitution kinetics—including but not limited to the following: *trans* effect/influence, Hammett parameter effects and secondary coordination sphere effects.[2] However, less explored in coordination chemistry are the kinetic effects of the flexibility, geometric fluxionality and molecular dynamics

Department of Chemistry, The University of Texas at Austin, 105 E 24th St, Austin, TX 78712, USA. E-mail: mrose@cm.utexas.edu

†Electronic supplementary information (ESI) available. CCDC 2181543 and 2181544. For ESI and crystallographic data in CIF or other electronic format see DOI: https://doi.org/10.1039/d2dt04048d

of metal complexes (and their coordination environments) on elementary substitution processes.

In the realm of organometallic catalysis the rigidity (or flexibility) of the catalytic system has, in fact, been considered to a limited extent. Powell studied turnover rates and selectivities for rhodium-based hydroformylations featuring diphosphine chelates of varying bite angles. The metal chelated by a BISBI ligand (a biaryl framework, Chart 1) ligand resulted in the highest selectivity for straight-chained aldehyde formation (66.5 $n:i$ ratio). Molecular mechanics calculations suggested the flexible BISBI ligand exhibited a *natural* bite angle of 113°, and a wide range of *thermally accessible* bite angles of 92°–155° within a 3 kcal mol^{-1} barrier of thermally added strain energy. The authors concluded that the natural bite angle alongside its range of flexibility contributed to the formation of an equatorial–equatorial intermediate that was ideal for generating linear aldehydes.[3] Further studies conducted by van Leeuwen considered the catalyst integrity of Rh-catalyzed hydroformylations by comparing systems supported by BISBI with those supported by rigid 'anthranoid' chelates (Xantphos, Sixantphos, Thixantphos; Chart 1) at elevated temperatures. Results indicated that the more rigid systems provided higher straight-chained aldehyde selectivities at 80 °C, as well as 40 °C—albeit with marginal selectivity in the latter case. The authors attributed this result to the increased stability of the rhodium center chelated by the more rigid 'anthranoid' ligand family.[4] Another notable result was that the turnover frequencies of the flexible BISBI complexes were higher at both temperatures, possibly indicating that the more flexible complexes are inherently more reactive than their rigid counterparts. However, no direct measurements of simple ligand exchange reactions were reported to underpin the more complicated *prima facia* catalytic results.

On this basis, we devised a scaffold-based approach to study the kinetic effects of molecular flexibility on the small molecule scale. We seek to understand the effects of flexibility and molecular dynamics on elementary ligand substitution reactions. More specifically, we desired to correlate ligand/complex flexibility with the kinetic parameters associated with ligand exchange. We recently reported the synthesis and structures of several coordination systems (Mn, Re and Fe carbonyls) supported by anthracene-based chelates. For example, Manes *et al.* reported the synthesis and structures of manganese tricarbonyl complexes ligated by bidentate anthracene-scaffold chelates (bis-pyridine, bis-thioether, mixed pyridine/thiolate).[5] The presence of the distal scaffold unit provides an ideal, modular approach to imbue a higher extent of molecular motion while retaining an identical primary coordination sphere—without disturbing the geometry, donor strength or other electronic qualities at the metal center.

In this work, in lieu of the rigid anthracene scaffold we have installed the more flexible and dynamic thianthrene scaffold (Chart 2) to impart greater flexibility to the related manganese carbonyl complex. In X-ray crystallographic studies, thianthrene exhibits a dihedral angle of 128°, representative of its 'butterfly' like geometry in the solid state.[6] However, thianthrene does not remain confined to this conformation in solution. Mazzanti reported the ring inversion dynamics of substituted thianthrene dioxide and tetraoxide *via* variable temperature ^{13}C NMR, which elucidated energetic barriers of 9.35 ± 0.15 kcal mol^{-1} and 6.50 ± 0.15 kcal mol^{-1}, respectively.[7] Another report by Ortiz elucidated ring inversion of thianthrene-5-oxide between equatorial and axial pseudo-boat conformations by extrapolating variable temperature ^{1}H NMR data of *trans* and *cis* thianthrene dioxide;[8] the ring inversion has a calculated activation energy of 3.8–7.4 kcal mol^{-1}. Thus, it is evident that thianthrene is quite dynamic in solution and we hypothesized that incorporation of the thianthrene scaffold as a comparison to the rigid anthracene scaffold would enable exploration of the influence of flexibility and molecular dynamics on the rates of ligand substitutions. The inherently stable $Mn(CO)_3$ unit provides an ideal and stable starting point for initiating ligand exchange reactions. Recently, Subramaniyan *et al.* published elegant work detailing the effect of ligand scaffold strain on the binding properties of

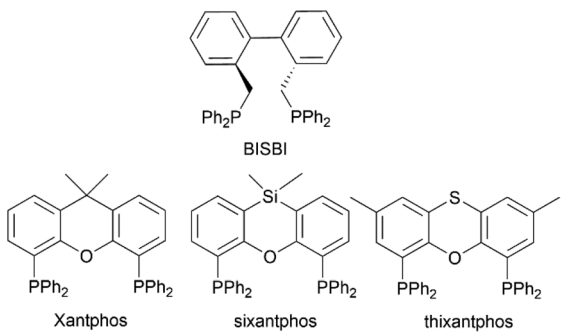

Chart 1 Structures of the ligands BISBI (top) and Xantphos, Sixantphos and Thixantphos (bottom).

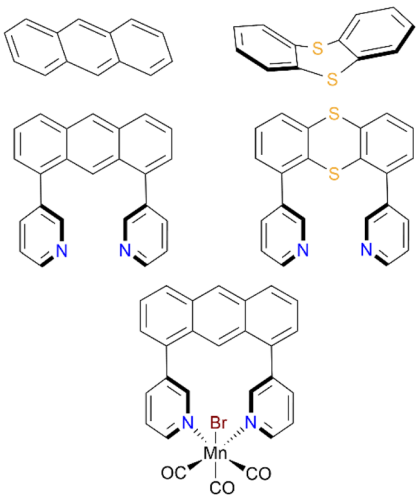

Chart 2 (Top) anthracene and thianthrene scaffolds, indicating their planarity or bent geometries in the solid state; (middle) previously synthesized anthracene-based,[5] and herein analogous thianthrene-based ligands; (bottom) previously synthesized anthracene-based complex.

PSP pincers. Three different PSP pincers of varying flexibility (thioxanthone, thioxanthene, and thioether-based) were employed to generate mononuclear κ^3-P,S,P palladium complexes resulting in differing internal ligand strains. DFT calculations accompanied by experimental results revealed that the formation of a dimeric species with an added equivalent of Pd, and the rapid ligand exchange of the thioxanthone-based pincer with the other two pincers were driven by the relief of internal ligand strain.[9] These results exemplify that ligand strain/flexibility can affect the energetic properties of metal complexes and should be properly considered.

Herein we report the synthesis of analogous, pyridine-based complexes featuring a thianthrene *versus* anthracene scaffold, and rates of PhCN → Br^- substitution reactions are compared between the rigid anthracene *versus* flexible thianthrene systems. Further evidence of the difference in molecular flexibilities is provided *via* ^{1}H NMR relaxation experiments, in that thianthrene-based compounds are more dynamic in solution than their anthracene counterparts.

Results and discussion

Ligand synthesis

Synthesis of the dibromothianthrene building block was derived from the works of Lovell, Sheikh and Ogawa.[10–12] As shown in Scheme 1, three synthetic steps produced **d** as the key intermediate that ultimately enabled a Suzuki cross-coupling to prepare the target symmetric ligand, **Thianth-py$_2$** (**1**). Beginning with thianthrene (**a**), selective mono-oxygenation of thianthrene (i) activated the 4 and 6 positions for lithiation and TMS insertion reaction. Oxygenation was performed with *meta*-chloroperoxybenzoic acid (*m*CPBA, 1.2 equiv.) at 0 °C to minimize side reactions (for example, generating thianthrene dioxide or tetroxide). For TMS insertion (ii), LDA was generated *in situ via* addition of *n*-BuLi to diisopropylamine. Distillation of ^{i}Pr$_2$NH was essential, as TMS insertion using commercial ^{i}Pr$_2$NH resulted in either no formation or only trace formation of **c**. The moderate yield of **c** (50%) is attributed to concomitant formation of mono- and tri-inserted TMS byproducts,[12] which were observed by ^{1}H NMR prior to purification. To subsequently produce the key coupling precursor **d**, a tandem one-pot bromination/reduction was employed.[10] After Br_2 treatment, addition of $Na_2SO_{3(aq)}$ both quenched unreacted Br_2 and deoxygenated (*i.e.* reduced) the sulfoxo moiety (85%). An alternative option was to perform a preceding deoxygenation with acetyl chloride, but we found the one-step process outlined by Sheikh to be more efficient. A Suzuki cross-coupling was performed to produce the desired ligand **Thianth-py$_2$** (**1**). An excess quantity of pyridine *meta*-boronic acid was added (3 equiv.) in ***iv*** to account for competing boronic acid reactions and possible degradation.[13]

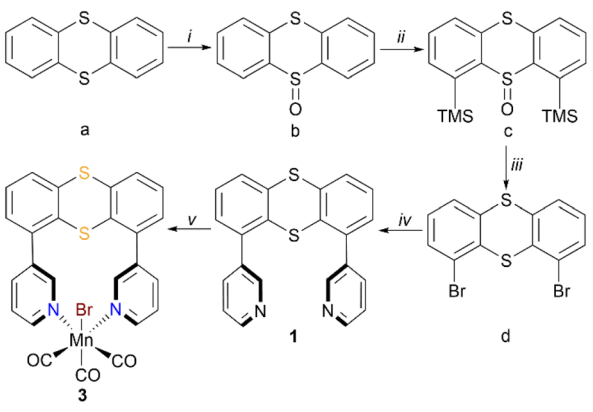

Scheme 1 Synthesis of **(Thianth-py$_2$)Mn(CO)$_3$Br (3)**: (i) *m*CPBA, 0 °C, DCM (72%); (ii) LDA, TMS-Cl, −78 °C, THF (50%); (iii) Br_2, $Na_2SO_{3(aq)}$, DCM, rt (85%); (iv) Na_2CO_3, pyridine-3-boronic acid, $Pd(PPh_3)_4$, reflux, 10 : 1 dioxane/H_2O (60%); (v) $Mn(CO)_5Br$, THF.

Ligand X-ray structures

The X-ray structure of **Thianth-py$_2$** (Fig. 1) was derived from crystals obtained *via* vapor diffusion of pentane into a DCM solution of the ligand. The thianthrene backbone exhibits a dihedral angle of 131° in the structure of **1**. This value deviates slightly from the 128° dihedral angle in the X-ray structure of thianthrene, itself, thus highlighting some range of flexibility of the scaffold. Likewise, the central C–S–C angle of **1** is 103°, which deviates from the 99° C–S–C angle of thianthrene. Regarding the orientation of the pyridine donor groups, **1** shares similar characteristics to its rigid anthracene counterpart **2**. First the rotation of the aryl units with respect to the scaffold minimizes steric clash between the donor arms. Second, the donor atoms (*N*) project outwards from the scaffold and in the same direction, favorable for facile metal complexation. Each pyridine moiety is tilted inwards (*N* atoms facing each other), with torsion angles of 60° or 78°. Such angles are comparable to the corresponding anthracene analog (62° or 64°). Thus, it is evident that the predominant difference between the thianthrene and anthracene-based ligands is the 'bent' *vs.* 'planar' geometry of the scaffold.

^{1}H NMR relaxation experiments

Relaxation is the restoration of nuclear spins to thermodynamic equilibrium. Specifically, spin–lattice (T_1) relaxation is the restoration of the net magnetization (vector sum) to the direction of the applied magnetic field, following an RF pulse

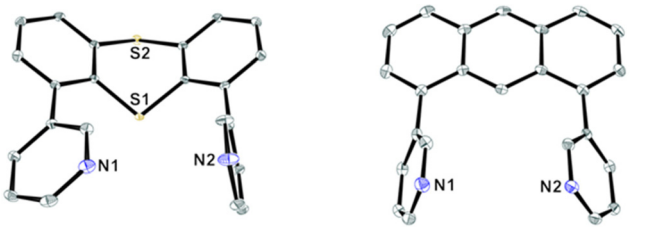

Fig. 1 ORTEP diagrams (30% thermal ellipsoids) of Thianth-py$_2$ (**1**, left) and Anth-py$_2$[5] (**2**, right); hydrogen atoms are omitted for the sake of clarity.

of a certain frequency. The applied RF pulse promotes nuclear spins to a high energy state, and for T_1 relaxation to proceed, the spins in the high energy state have to release/distribute energy to the lattice (neighboring molecules and atoms) and return to thermal equilibrium. The lattice (essentially molecular motions) will vary in frequency from molecule to molecule, and thus relaxation rates are strongly affected by the tumbling rate of a molecule in solution.[14] Relaxation will proceed swiftly if the frequency of tumbling corresponds to the energy gap between the high energy and equilibrium states. Naturally, if the tumbling frequency does not correspond to this energy gap, relaxation will proceed at a slower rate; this is observed with very large macromolecular systems such as proteins (slow tumbling) and conversely with small, single molecules (fast tumbling).

Because of the strong correlation between molecular motion and relaxation rates, NMR relaxation experiments are a common method to probe the localized dynamics of protein structures.[15,16] For this reason, we performed T_1 ^{1}H NMR relaxation experiments on the analogous flexible and rigid ligands (**1** and **2**, respectively) and specifically analyzed the scaffold protons indicated in Fig. 2. The relaxation experiments were carried out at the same temperature (25 °C) and concentration (15 mM). The overall tumbling frequencies and corresponding relaxation rates between the analogous ligands are expected to be comparable because of the similar ligand sizes.

Table 1 displays the resulting T_1 relaxation times for the scaffold protons of **1** and **2**. Notably, proton α for **Thianth-py$_2$** and **Anth-py$_2$** have relaxation times of 2.97 s and 1.91 s, respectively. The remaining scaffold protons share comparable relaxation times (data fits can be found in ESI, Fig. S7 and S8†). Though the overall tumbling of the analogous ligands was expected to be the same, intramolecular motions can affect T_1 relaxation bearing that the motions are of similar time scale as the tumbling. Li *et al.* performed ^{13}C T_1 relaxation experiments on the β-carotene related molecules squalene and squalane. Results indicated that the exterior carbons exhibited longer relaxation times (~3 s) than the internal carbons. The carbons on the molecular perimeter experience fast rotations around the bond that is on the same order of the overall tumbling of the molecules, thus the relaxation times are longer.[17] Intramolecular, librational motions of molecules can also affect T_1 relaxation. Williams *et al.* performed ^{2}H T_1 relaxation experiments on secondary amides, which present an out-of-plane librational motion that strongly affects relaxation rates.[18] The amides with more prominent (fast) librational motions resulted in longer ^{2}H T_1 relaxation times.

Assessing thianthrene, the flapping motion can be defined as a librational motion about the center sulfur atoms. The α proton of **1** is in close proximity to the origin of libration and thus exhibits a longer relaxation time than the α proton of **2**, which does not contain the same librational motion. This result leads to two conclusions: the thianthrene scaffold incorporates flexibility to the ligand in the form of 'flapping', and this motion is on the timescale of the overall tumbling of the molecule.

Metal complexation

The complexation of **Thianth-py$_2$** with $Mn(CO)_5Br$ proceeded smoothly in THF to form [(Thianth-py$_2$)$Mn(CO)_3Br$] (**3**). The IR spectra presented in Fig. 3 each feature three CO stretches as a result of the C_S symmetry of both complexes. Importantly, the stretching frequencies are nearly identical between **3** and **4**, indicative of similar electronic properties at the Mn center. Unfortunately, the well-known problem of resonance broadness in the ^{1}H NMR spectra of the corresponding manganese complexes (presumably due to ^{55}Mn, I = 5/2) precluded acquisition of T_1 times for the metal complexes—despite their low-spin, d^6 diamagnetism.

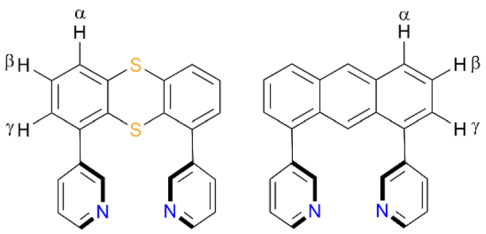

Fig. 2 Ligand structures indicating the scaffold protons on which T_1 analysis was performed, with corresponding labeling scheme.

Table 1 ^{1}H NMR relaxation times (s) for Thianth-py2 (**1**) and Anth-py2 (**2**)

Proton	Thianth-py$_2$ (**1**)	Anth-py$_2$ (**2**)
α	2.97	1.91
B	1.91	1.89
λ	2.35	2.22

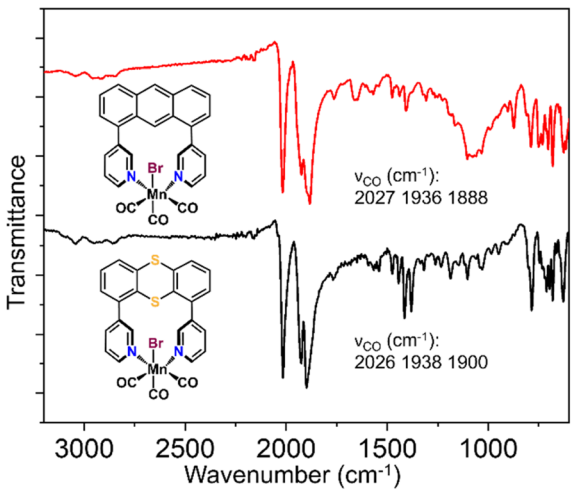

Fig. 3 IR spectra of [(Anth-py$_2$)$Mn(CO)_3Br$] (**4**) (red trace) and [(Thianth-py$_2$)$Mn(CO)_3Br$] (**3**) (black trace) with corresponding CO stretching frequencies.

X-ray structures of manganese complexes

Fig. 4 depicts the ORTEP diagrams from the X-ray structures of [(Thianth-py_2)Mn$(CO)_3$Br] (**3**) and [(Anth-py_2)Mn$(CO)_3$Br] (**4**). Both structures exhibit pseudo-octahedral geometries with the chelating pyridine donors and bromide arrayed in a facial manner, and the opposing face is occupied by the three CO ligands in piano-stool fashion. The full crystal structure of **3** (Fig. S6†) exhibits disorder between the axial CO and Br ligands, with 87% occupancy of Br at the apical position and 13% occupancy in the bottom position (CO occupancies are *vice versa*). The thianthrene scaffold in **3** exhibits a 146° dihedral angle, compared to 131° in the free ligand. The 15° difference highlights the flexibility of thianthrene. As listed in Table 2, there is a 19° difference between the torsion angles of **3** and **4**. Due to the 'bent' thianthrene conformation, the pyridine units of **1** do not require rotation to the same extent necessary in its anthracene counterpart to bind the Mn center: the arms of the Thianth-py_2 ligand of **3** require a 5° inward rotation, while the arms of the Anth-py_2 ligand of **4** require a 20° inward rotation with respect to the ~65° torsion present in both free ligands **1** and **2**. Another notable feature is that the central sulfur atom in the thianthrene scaffold does not directly interact with the Mn center, as evidenced by an Mn1···S1 distance of 5.36 Å in **3**. The remaining bond distances and angles of interest are displayed in Table 2 and are very similar between the corresponding systems. Considering the similar bond metrics and C≡O stretching frequencies, it is evident that the analogous thianthrene and anthracene Mn complexes are electronically very similar. Therefore—and critically—on the basis of both spectroscopic and X-ray structural parameters, we conclude that the exclusive distinguishing feature of molecular flexibility should account for any substantive reactivity differences between the analogous systems.

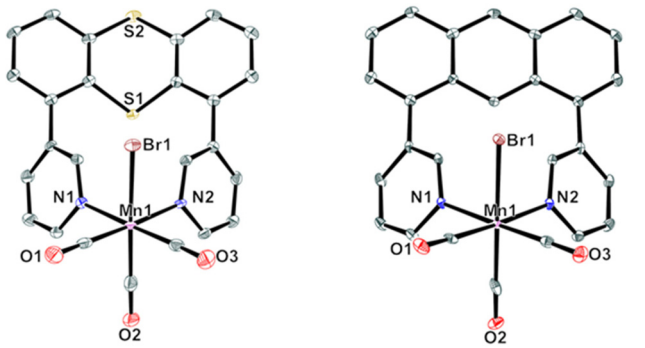

Fig. 4 ORTEP diagrams (30% ellipsoids) of [(Thianth-py_2)Mn$(CO)_3$Br] (**3**, left) and [(Anth-py_2)Mn$(CO)_3$Br] (**4**, right); hydrogen atoms are omitted for clarity.

Table 2 Comparison of selected bond distances (Å) and bond angle (°) for the complexes **3** and **4**

Complex	3	4
Mn–N1	2.129(5)	2.135(3)
Mn–N2	2.116(4)	2.118(3)
Mn–CO	1.818(6)	1.818(4)
	1.802(7)	1.837(4)
	1.794(6)	1.800(4)
Mn–Br	2.518(8)	2.522(6)
Bite angle	86.7(2)	90.38(10)
Torsion angle	65(7)	46(4)

Ligand exchange kinetics

Our aim was to use vibrational spectroscopy to monitor a ligand exchange reaction with the pair of manganese complexes. We first attempted performing CO → L (L = neutral ligand) substitution reactions, aiming to monitor the disappearance of a characteristic metal carbonyl stretch. Unfortunately, all attempts at controlled decarbonylation resulted in either no reaction or uncontrollable CO exchange (loss of all CO ligands). For example, treatment of **3** with trimethylamine-*N*-oxide (TMAO) in THF resulted in no reaction, highlighting the inherent stability of the Mn tricarbonyl motif.

Another attempt was Br^- abstraction with $AgBF_4$ to form the species [Mn(Thianth-py_2)$(CO)_3$THF](BF_4) (ν_{CO} ≈ 2045, 1951, 1927), followed by treatment of the resulting cation with TMAO. However, the cation proved too electrophilic, and the uncontrolled loss of all CO ligands was observed. We also subjected **3** to UV light [long wave (λ = 350 nm) and short wave (λ = 250 nm)] in THF, again resulting in uncontrolled loss of all CO ligands.[19,20] Based on the results, we hypothesized that the stability of the tri/di-carbonyl motif is drastically decreased upon loss of one CO ligand, thus leading to rapid decomposition.

We thus attempted Br^- → L ligand exchanges, resulting in the successful and trackable (back) reaction displayed in Scheme 2. Treatment of **3** with $AgBF_4$ generates the Br^- abstracted cation **5** which can be subsequently treated with

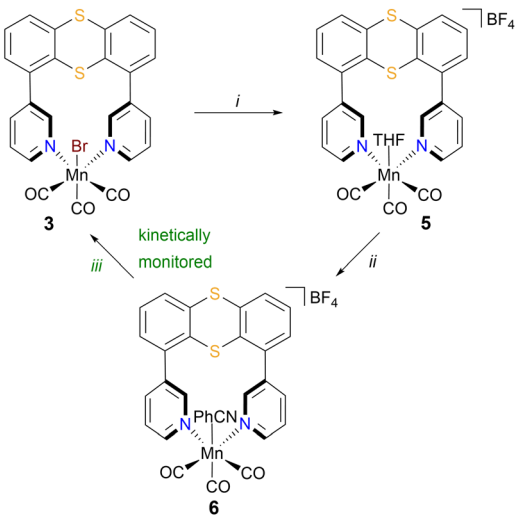

Scheme 2 Ligand exchange reaction scheme for bromide abstraction and kinetic monitoring (green): (i) $AgBF_4$, THF; (ii) PhCN in THF; (iii) tetraoctylammonium bromide in THF.

benzonitrile (PhCN) to form the stable species **6**. This complex was then successfully 'back-substituted' (with kinetic monitoring) to the original compound **3** *via* treatment with tetra-octylammonium bromide (TOAB) in THF. The identical reaction conditions were applied to the rigid system [(Anth-py_2)Mn$(CO)_3$Br] (**4**) to navigate the same reaction cycle. We note that the reverse reaction for (i) with TOAB was attempted and resulted in rapid ligand exchange combined with oxidation of the Mn center and loss of CO ligands. For this reason, the more stable PhCN adduct was generated. Fig. S9† displays the IR spectra and resulting CO frequency shift of the kinetically monitored ligand exchange (iii). The reaction from the PhCN-bound species back to the Br^- bound species results in a nearly identical shift of CO stretching frequencies for both the thianthrene and anthracene-scaffolded compounds. These similarities further enforce the comparable electronic properties of the manganese center between the two systems.

With a successful and trackable ligand exchange reaction in hand, kinetic data was obtained to compare reaction rates of PhCN → Br^- ligand substitution for the flexible thianthrene-based complex **3** *versus* the rigid anthracene-based complex **4**. Initiating the ligand exchange at 0 °C slowed the reaction to enable IR monitoring, and the resulting kinetic plot is displayed in Fig. 5. As indicated in Table 3, the initial 0° C reaction rate for the thianthrene-based complex (k = 43.3 × 10^{-3} min^{-1}; $t_{\frac{1}{2}}$ = 16.00 min) is ~5× faster than the corresponding anthracene-based kinetics (k = 9.03 × 10^{-3} min^{-1}; $t_{\frac{1}{2}}$ = 76.76 min). Furthermore, the exponential decay plots (ESI, Fig. S11 and S12†) emphasize the stark difference in total time to >95% reaction completion: thianthrene: t_{comp} = 37 min; anthracene system: t_{comp} = 85 min.

The data clearly conclude that the more flexible, thianthrene-based complex accomplishes PhCN → Br^- ligand exchange at a faster rate than the rigid, anthracene-based complex. We also experimentally determined that there is a 1st order [Br^-] dependence on the ligand exchange: With compound **6**, the reaction was performed with 2 or 4 equivalents of TOAB, resulting in total time to >95% reaction completion of 23.5 min and 13.5 min, respectively. The kinetic plots of the 'room temperature' region can be found in the ESI (Fig. S13†).

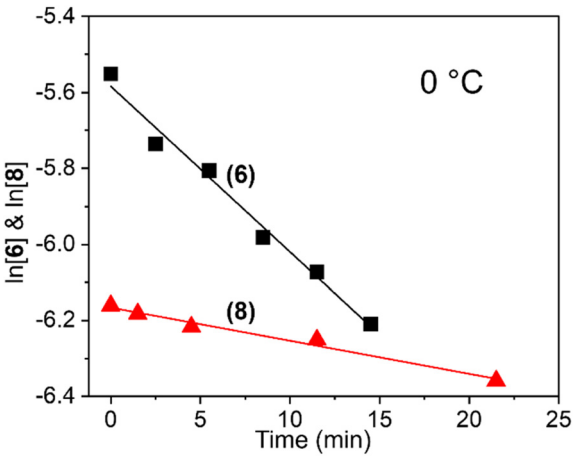

Fig. 5 Kinetic plot of (iii) at 0 °C. The black squares depict the reaction with **6** ([(Thianth-py_2)Mn$(CO)_3$PhCN](BF_4)) and the red triangles depict the reaction with **8** ([(Anth-py_2)Mn$(CO)_3$PhCN](BF_4)).

Table 3 Displayed are the reaction times along with the corresponding rate constants for the formation of **3** and **4**; all data is the average ± s.d. of two trials

Complex	3	4
>95% complete (min)	37.50 ± 3.53	85.00 ± 5.66
0 °C k_{obs} (min^{-1})	43.33 × 10^{-3} ± 0.0038	9.03 × 10^{-3} ± 0.00192
0 °C $t_{1/2}$ (min)	16.00 ± 1.41	76.76 ± 16.68

Constrained scaffold angle geometry optimizations and energy analysis

Constrained angle DFT calculations were performed on the geometry optimized structures of **1**, **2**, **3** and **4** to elucidate the range of dihedral angles that the scaffolds can accommodate with energies commensurate to kT at ambient temperatures. A computational scan was performed at varying constrained (scaffold) dihedral angles, and the remaining atoms of the compounds were allowed to relax to their energy-minimized coordinates. This calculation resulted in the parabolic energy curves depicted in Fig. 6. The geometry-optimized structure of **3** exhibits a 140° dihedral angle that, remarkably, can widely vary from a more acute angle (~133°) to an obtuse angle (~148°) within kT of ambient temperature (0.6 kcal mol^{-1}). Deviation from a dihedral angle of more than ~10° in either direction (acute or obtuse) results in geometric strain in **3**, and the energy increases exponentially. The same calculation was performed on the corresponding free ligand (**1**) to observe how restricted the 'flapping' motion of the scaffold becomes upon metal binding. Results indicate that the range of reasonably accessible scaffold dihedral angles at ambient temperature is larger for the free ligands **1** and **2** than within their manganese complexes **3** and **4**, but importantly the flexibility is not completely mitigated upon complexation. The irregularities in the 'valley' of the **1**'s energy profile are due to steric clashes in the freely rotating pyridine arms, which are otherwise fixed in the case of complex **3**. DFT calculations on the more rigid, anthracene ligand and corresponding complex resulted in a much narrower range of ~7° (172°–179°) and ~5° (176°–181°), respectfully at 0.6 kcal mol^{-1}.

To illustrate the compensatory motions of **3** in the rest of the structure upon geometry optimization at different fixed angles, selected structural metrics are plotted as a function of scaffold dihedral angles. Plots of scaffold angle *versus* M–L bond distances were constructed to evaluate the effect of scaffold motion on the primary coordination sphere (Fig. S16†). These reveal *no change of bond metrics* over the course of scaffold distortion. However, to compensate for the persistent M–L bond lengths and angles, the pyridine 'arms' of **3** systematically rotate within a range of 6° (from 62°–68°) within the scaffold dihedral angle range of 133°–148° (Fig. 7).

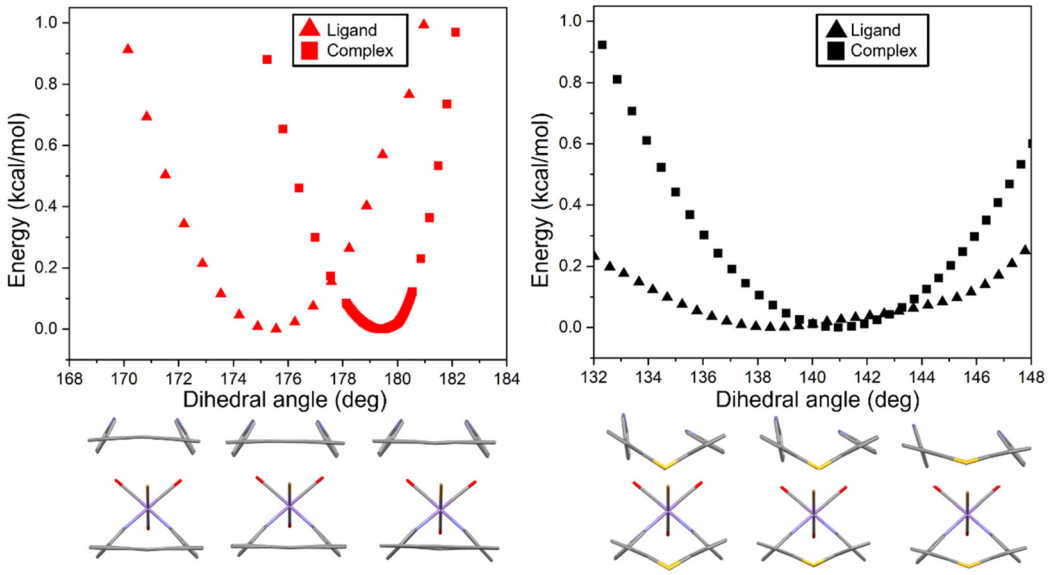

Fig. 6 Plots of the DFT constrained scaffold angle scan for **2** and **4** (left) and **1** and **3** (right). Selected structures at the extremes and median of the *kT* range are depicted beneath the corresponding plots. The full plots can be found in Fig. S15.†

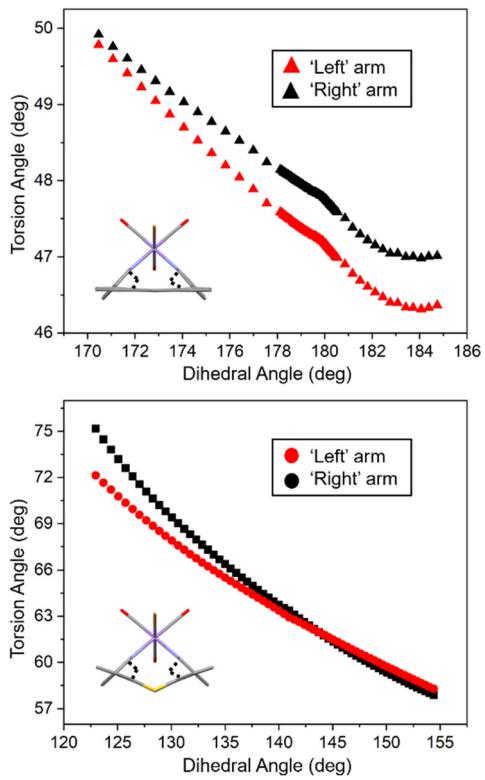

Fig. 7 Plots of the DFT scaffold dihedral angle scan *versus* the torsion angle of the pyridine units for **3** (bottom) and **4** (top).

This rotational motion is perhaps the key point of flexibility that enables the metal complex geometry to remain invariant despite the significant scaffold bending angle. It is worth noting the smaller rotational range of 1° for **4** within the scaffold dihedral angle range of 176°–181°, resulting from the increased scaffold rigidity.

Discussion

With the result of the constant M–L bond distances as the thianthrene scaffold 'flaps', the increased ligand exchange rate for the flexible thianthrene-based complex is likely not thermodynamically (ΔG) explained. At a given temperature, the structural metrics within the first coordination spheres of the Thianth and Anth-based species are similar.

In the discussion below, our goal is to outline several possible lines of reasoning to explain the correlation between enhanced molecular flexibility and accelerated reaction rates. Our intent is not at present to identify which of the delineated rationale(s) is most applicable to this system, or in general. We wish to survey the possibilities to place the present results in context, as well as provide a concrete direction for future studies and hypotheses. We note that the delineated explanations need not be mutually exclusive. All of the proposed kinetic arguments share the same root effect: namely, that flexibility offers a greater range of structural geometries, which can increase the rate of reactions through several mechanisms.

Rationale A: breadth of transition state saddle point

As previously mentioned, the structural and spectroscopic characterization demonstrates that the electronic properties at the manganese center are nearly identical between the thianthrene- and anthracene-based complexes, and thus we attribute the observed reactivity differences to the enhanced flexibility of the thianthrene scaffold. The more flexible complex

has access to more varied geometries (greater number of microstates), leading to a higher chance of a geometrically conducive environment for the reaction to proceed. More specifically, this rationale can manifest along the reaction pathway in terms of the transition state. For example, reactions possess optimal (as well as non-optimal) transition state structures for the reaction to proceed (Fig. 8, left). The low-energy saddle point at the transition state for a rigid system is represented as a narrow parabola (Fig. 8, top), and thus has limited thermal access (within kT) to slight variations in geometry that can proceed through the lowest (or near-lowest) optimal transition state geometries at comparable rates; this results in an overall slow rate of reaction.

In contrast, the saddle point at the transition state for a flexible system (Fig. 8, bottom) is represented as a broad parabola. As a result, highly flexible systems retain thermal access (within kT) to a variety of low-energy, slightly varied geometries (geometrically variant, but not energetically strained) that can pass through the broad transition state saddle point at comparably low energies. Hence, the reaction can proceed along different trajectories with minimal additional energy. This rationale mirrors the well-known argument in the literature of conformational sampling leading to enhanced rates of catalysis within enzymes.[22] Vazquez *et al.* elucidated that a multipath formulation of variational transition-state theory provided a more accurate kinetic view (along with rate constants) for the decomposition of 1-propanol radicals.[21] Essentially, this work demonstrated that multiple transition-state conformers contribute to the overall reaction rates, and taking this into account provides more accurate results than an approach focused on the most stable/optimized conformer. The aforementioned result can be extended to our rationale: if

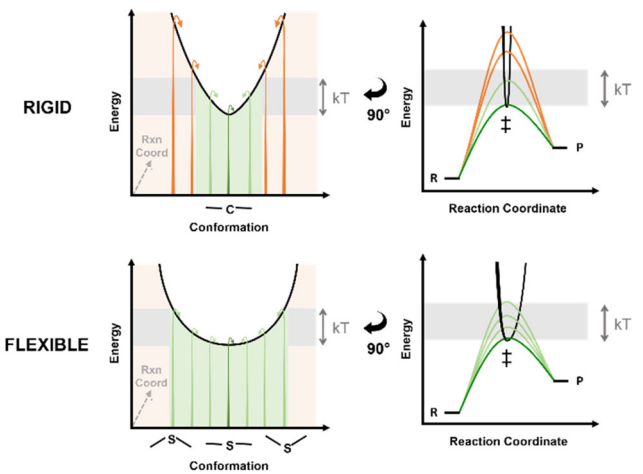

Fig. 8 Rationale A: transition state saddle point comparison of a rigid (top) *vs.* flexible (bottom) structure. The grey highlighted region represents a small energy range above the optimal reaction trajectory (dark green arrow). The light green arrows represent the individual reaction trajectories possible within the grey highlighted energy range. The respective saddle point comparisons are depicted as a 2-D reaction coordinate.

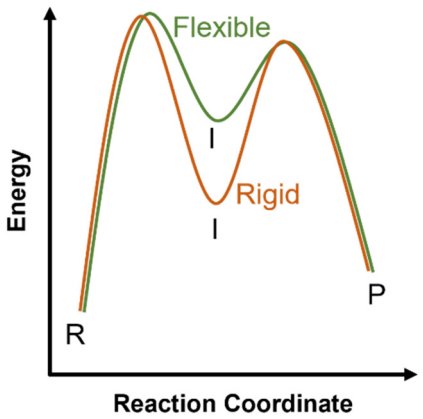

Fig. 9 Rationale B: simple reaction coordinate diagram comparing the access to strained intermediate structure and geometries for rigid systems (orange trace) and flexible systems (green trace).

multiple transition-state conformers contribute to the overall reaction rate, and a more flexible compound can access more geometric variations at low energy expenses, the resultant reaction rate can effectively be faster compared to an analogous, rigid compound.

Rationale B: modulated energy of intermediates

Another key aspect that affects reaction kinetics is the formation of intermediates along the reaction pathway. As expected, more stabilized intermediates will result in slower overall reaction kinetics, while destabilized intermediates can result in faster overall reaction kinetics, bearing that the destabilization does not pose a large energy penalty. The 'destabilization intermediate effect' has been observed with the enzyme human transkeltotase (hTK). Crystal structures of the reaction intermediates reveal an out-of-plane distortion (20°) of the covalent bond linking the cofactor and substrate. This distortion results in a small energy penalty (0.2 kcal mol^{-1}) as shown by QM/MM calculations.[22] The intermediate structure, which precedes a TS, is prevented from residing in an energy well and subsequently decreases the TS energy barrier, resulting in a more efficient process.[23,24] The enzyme's flexible nature allows the bond distortion and resultant destabilization, and the same effect can plausibly manifest within small-molecule systems. For example, a flexible structure can access more highly strained intermediate structures and geometries (Fig. 9, green trace) compared to an analogous, rigid structure (Fig. 9, orange trace)—thus leading to faster overall reaction kinetics.

Conclusions

In summary we have synthesized a scaffold-variable system in which direct comparisons can be made between complexes with the same coordination donors and environment, and nearly identical electronic structure and zero-point geometries (around the metal center), but nevertheless possess different

capacities for molecular flexibility. The thianthrene-based family of complexes like **3** and the anthracene-based family of complexes like **4** exhibit essentially indistinguishable IR spectra (ν_{CO} region) and structural metrics, yet display vastly different functional kinetics. The flexible thianthrene family of **3** exhibits 4–5× faster kinetics in ligand substitution reactions than the rigid anthracene family of **4**. We attribute the accelerated reaction kinetics for the thianthrene-based system to its enhanced flexibility. Future experimental and computational work must explore the competing (or synergistic) rationales regarding reaction pathway energetics to further understand the critical role that molecular flexibility plays in imparting reactivity to coordination complexes, organometallics and biological metalloenzyme sites.

Author contributions

Methodology: J. Labrecque, Y. I. Cho, D. K. McIntosh; investigation: J. Labrecque, Y. I. Cho, F. Agboola; writing: J. Labrecque, M. J. Rose; supervision: M. J. Rose.

Conflicts of interest

There are no conflicts of interest.

Acknowledgements

We acknowledge funding from the National Science Foundation (NSF-CHE 2109175) and the Robert A. Welch foundation (F-1822). We thank Dr Vince Lynch for assistance in X-ray data collection and structure refinement. We also thank Professor Carlos Baiz and Zireena Al-Mualem for assistance in infrared spectroscopic studies.

References

1 F. Basolo and G. R. Pearson, *Mechanisms of Inorganic Reactions: A Study of Metal Complexes in Solution*, John Wiley and Sons, Inc., New York, 1967, p. 701.
2 R. L. Shook and A. S. Borovik, The Role of the Secondary Coordination Sphere in Metal-Mediated Dioxyden Activation., *Inorg. Chem.*, 2010, **49**(8), 3646–3660.
3 C. P. Casey, G. T. Whiteker, M. G. Melville, L. M. Petrovich, J. A. Gavney Jr. and D. R. Powell, Diphosphines with Natural Bite Angles near 120° Increase Selectivity for n-aldehyde Formation in Rhodium-Catalyzed Hydroformylation, *J. Am. Chem. Soc.*, 1992, **114**(14), 5535–5543.
4 M. Kranenburg, Y. E. M. van der Burgt, P. C. J. Kramer, P. W. N. M. van Leeuwen, K. Goubitz and J. Fraanje, New Diphosphine Ligands Based on Heterocyclic Aromatics Inducing Very High Regioselectivity in Rhodium-Catalyzed Hydroformylation: Effect of the Bite Angle, *Organometallics*, 1995, **14**(6), 3081–3089.
5 T. A. Manes and M. J. Rose, Mono and Dinuclear Manganese Carbonyls Supported by 1,8-Disubstituted (L=Py, S_{Me}, S_H) Anthracene Ligand Scaffolds, *Inorg. Chem.*, 2016, **55**(11), 5127–5138.
6 S. B. Larson, S. H. Simonsen, G. E. Martin, K. Smith and S. Puig-Torres, Structures of Thianthrene (I), $C_{12}H_8S_2$, (redetermination at 163 K and 295 K) and 1-azathianthrene (II), $C_{11}H_7S_2$, (at 163 K), *Acta Cryst.*, 1984, **C40**, 103–106.
7 D. Casarini, C. Coluccini, L. Lunazzi and A. Mazzanti, Ring Inversion Dynamics of Derivatives of Thianthrene Di- and Tetraoxide, *J. Org. Chem.*, 2006, **71**(16), 6248–6250.
8 M. E. Gonzalez-Nunez, R. Mello, J. Royo, G. Asensio, I. Monzo, F. Tomas, J. G. Lopez and F. L. Ortiz, Conformational Mobility of Thianthrene-5-oxide, *J. Org. Chem.*, 2005, **70**(9), 3450–3457.
9 V. Subramaniyan, F. Tibika and Y. Tulchinsky, Effect of Internal Ligand Strain on Coordination Behavior of PSP Pincer Ligands, *Inorg. Chem.*, 2023, **62**(1), 123–136.
10 J. M. Lovell, R. L. Beddoes and J. A. Joule, Synthesis of 4,6-Disubstituted Thianthrenes, X-ray Crystal Structures of 4,6-Diphenylthianthrene and 1-Tetrathiafulvalenylnaphthalene, *Tetrahedron*, 1996, **52**(13), 4745–4756.
11 M. C. Sheikh, T. Iwasawa, A. Nakajima, A. Kitao, N. Tsubaki, R. Miyatake, T. Yoshimura and H. Morita, Synthesis of Thianthrene Derivatives Linked by Carbon Chains, *Synthesis*, 2014, **46**(1), 42–48.
12 S. Ogawa, H. Muraoka and R. Sato, Design of Reversible Organic-Organometallic Multi-redox Systems Using Thianthrene Having Ferrocene Fragments, *Tetrahedron Lett.*, 2006, **47**(15), 2479–2483.
13 A. J. J. Lennox and G. C. Lloyd-Jones, Selection of Boron Reagents for Suzuki-Miyuara Coupling, *Chem. Soc. Rev.*, 2014, **43**, 412–443.
14 J. Keeler, *Understanding NMR Spectroscopy*, John Wiley and Sons, Inc, England, 2010, p. 245.
15 A. G. Krushelnitsky and V. D. Fedotov, Overall and Internal Protein Dynamics in Solution Studied by the Nonselective Proton Relaxation, *J. Biomol. Struct. Dyn.*, 1993, **11**(1), 121–141.
16 Y. Chen, S. L. Campbell and N. V. Dokholyan, Deciphering Protein Dynamics from NMR Data Using Explicit Structure Sampling and Selection, *Biophys. J.*, 2007, **93**(7), 2300–2306.
17 S. Li, S. L. Swindle, S. K. Smith, R. A. Nieman, A. L. Moore, T. A. Moore and D. Gust, Molecular Motions of β-Carotene and a Carotenoporphyrin Dyad in Solution: A carbon-13 NMR Spin-Lattice Relaxation Time Study, *J. Phys. Chem.*, 1995, **99**(10), 3371–3378.
18 J. C. Williams and A. E. McDermott, Variable NMR Spin-Lattice Relaxation Times in Secondary Amides: Effect of Ramachandran Angles on Librational Dynamics, *J. Phys. Chem. B*, 1998, **102**(32), 6248–6259.
19 S. Pai, M. Hafftlang, G. Atongo, C. Nagel, J. Niesel, S. Botov, H. G. Schmalz, B. Yard and U. Schatzschneider, New Modular Mangenese(I) Tricarbonyl Complexes as PhotoCORMs:

in vitro Detection of Photoinduced Carbon Monoxide Release Using COP-1 as a Fluorogenic Switch-on Probe, *Dalton Trans.*, 2014, **43**, 8664–8678.

20 S. J. Carrington, I. Chakroborty and P. K. Mascharak, Exceptionally Rapid CO Release from a Manganese(I) Tricarbonyl Complex Derived from Bis(4-chloro-phenylimino)acenaphthene Upon Exposure to Visible Light, *Dalton Trans.*, 2015, **44**, 13828–13834.

21 D. Ferro-Costas, E. Martinez-Nunez, J. Rodriguez-Otero, E. Cabaleiro-Lago, C. M. Estevez, B. Fernandez, A. Fernandez-Ramos and S. A. Vazquez, Influence of Multiple Conformations and Paths on Rate Constants and Product Branching Ratios. Thermal Decomposition of 1-Propanol Radicals, *J. Phys. Chem. A*, 2018, **122**(21), 4790–4800.

22 S. Hammes-Schiffer, Catalytic Efficiency of Enzymes: A Theoretical Analysis, *Biochemistry*, 2013, **52**(12), 2012–2020.

23 S. Ludtke, P. Neumann, K. M. Erixon, F. Leeper, R. Kluger, R. Ficner and K. Tittmann, Sub-Angstrom-Resolution Crystallography Reveals Physical Distortions that Enhance Reactivity of a Covalent Enzymatic Intermediate, *Nat. Chem.*, 2013, **5**, 762–767.

24 M. Prejano, F. E. Medina, M. J. Ramos, N. Russo, P. A. Fernandes and T. Marino, How the Destabilization of a Reaction Intermediate Affects Enzymatic Efficiency: The case of Human Transketolase, *ACS Catal.*, 2020, **10**(4), 2872–2881.